IEEE Access
Multidisciplinary | Rapid Review | Open Access Journal

Received July 15, 2020, accepted July 21, 2020, date of publication July 30, 2020, date of current version August 18, 2020.

Digital Object Identifier 10.1109/ACCESS.2020.3013137

Immersion and Invariance Manifold Adaptive Control of the DC-Link Voltage in Flywheel Energy Storage System Discharge

LEI GONG, MENG WANG, AND CHANGSHENG ZHU
College of Electrical Engineering, Zhejiang University, Hangzhou 310027, China
Corresponding author: Changsheng Zhu (zhu_zhang@zju.edu.cn)

This work was supported in part by the National Key Research and Development Program of China under Grant 2018YFB0905500, and in part by the National Natural Science Foundation of China under Grant 11632015.

ABSTRACT In order to keep constant DC-link voltage of a flywheel energy storage system (FESS) discharge in a wide rotational speed range, the control structure of the FESS is comprised of an inner current loop and an outer DC-link voltage loop. Since the dynamic equation of the DC-link voltage in the FESS discharge is nonlinear, it is difficult for some controllers to make the DC-link voltage in discharge be constant as the rotational speed is varying in a large range. Considering the nonlinearity of the DC-link voltage in discharge and the fast discharge requirements of the FESS, an immersion and invariance manifold (I&IM) adaptive nonlinear controller for a constant DC-link voltage is proposed via methodology of immersed in the invariant manifold. The stability of the control algorithm and the influence of the parameter error on the stability are verified by the Lyapunov stability theory, and the influence of the parameters error on the steady state and transient characteristics of the closed-loop system is analyzed numerically. It is proved that the closed-loop system satisfies the global uniform asymptotic stability conditions at the equilibrium point, and the error of the model parameters does not affect the equilibrium point of the system. Finally, the effectiveness of the I&IM adaptive nonlinear controller were studied by simulation and experiment. The results show that the DC-link voltage in discharge remains stable when switching the system load in cases of different rotational speeds and loads.

INDEX TERMS Flywheel energy storage system (FESS), bus voltage, immersion and invariance manifold (I&IM), Lyapunov stability, adaptive nonlinear controller.

I. INTRODUCTION

Flywheel energy storage system (FESS) is an energy storage system where mechanical energy is stored in a rotating flywheel that is integrated with a motor/generator and driven by a bidirectional power converter. It is very suitable in cases when discharge is often needed during a short period (tens of seconds) with medium to high power (kW to MW). Therefore, the FESS is a competitive candidate in the fields of energy recovery, micro grids, uninterruptible power supplies, renewable energy resource, etc. [1]–[3].

In practice, as a storage device saving mechanical energy from electrical energy, the integrated motor/generator is an essential part of the FESS, the exchange between electricity and mechanical energy is just relying on the accelerating and decelerating operation of the motor/generator. At present, several types of motor/generator are available for the FESS, among which the permanent magnet synchronous motor/generator (PMSM/G) is often chosen for its high efficiency, high power factor, high power density and good dynamic performance [4].

The motor used in the FESS should operate in wide rotational speed range due to its discharge mechanism, and the rotational speed sudden change in a short discharge period is a challenge for the controller design of the FESS. As the rotational speed varies, the amplitude and frequency of back electromotive force in the PMSM/G consecutively change. In order to provide proper amounts of instantaneous power, the active current has to be adjusted with relatively high dynamic property. For the controller design of the FESS

The associate editor coordinating the review of this manuscript and approving it for publication was Bohui Wang.

several advanced control methods have been proposed to achieve high-precision control performance. These methods include the sliding model control, the adaptive control, the internal model control, the active disturbance rejection control, etc.

Since the discharge status usually has a great influence on the performance of the FESS, keeping the DC-link voltage constant in discharge is a practical strategy to make the FESS track the power of the load devices as soon as possible. However, most published papers on the control of the FESS are focused on the torque current control [5]–[7] or cooperation with other parts of the system where the FESS is applied [8]–[11], whereas limited work has been done upon the underlying algorithm of the control of DC-link voltage in the discharge process.

It has been recognized that the dynamic behavior of the DC-link voltage in discharge based on a PWM rectifier is nonlinear, and various attempts have been made to deal with the nonlinearity with the common idea of designing a linear controller after accurate linearization [12], [13]. However, the accurate linearization is highly dependent on the accuracy of the model and parameters of the system, which cannot be obtained in practice, or too complex to implement in practice.

Some advanced adaptive control methods were proposed to control nonlinear systems. Liu *et al*. [14] proposed adaptive fuzzy output-feedback tracking control to estimate the unmeasurable states of the switched system, an appropriate stochastic Lyapunov–Krasovskii functional tackled the time-delay terms, and fuzzy logic systems were employed to approximate the unknown nonlinearities. Sousy *et al*. [15] proposed an adaptive nonlinear disturbance observer for identification and control of a two-axis motion control system driven by two permanent-magnet linear synchronous motors servo drives. Taghavifar *et al*. [16] estimated the nonlinear system dynamics using the universal approximation capacity of the neuro-fuzzy type-2 approach and the states were obtained by the adaptive robust state observer. Ma *et al*. [17] also proposed adaptive finite-time output-feedback control for a class of completely non-affine uncertain switched pure-feedback nonlinear systems with unmeasurable states. Chang *et al*. [18] studied the estimation problem for a class of nonlinear tunnel diode circuits with parameter perturbation. Kenny *et al*. [19] presented a novel control algorithm for the charging and discharging operation of FESS served as uninterruptible power supply for space application. Francisco *et al.* [8] put forward a new design and the experimental validation of an energy management algorithm for flywheel battery, aiming to smooth the power injected to the grid by a wind turbine. Chang *et al.* [20] studied a model-independent controller based on active disturbance rejection control for the bidirectional Buck–Boost converter control in the FESS, which can estimate and compensate model uncertainties and unknown disturbances in real time, but they do not focused on the effect of the wide-range speed variation. Fang *et al.* [21] studied charging and discharging control strategies for the FESS driven by switched reluctance machine. Zhang and Yang [22] proposed a robust discharge strategy to deal with the wide range speed variation and ensure a consistent robust discharge performance for the PMSM/G-based FESS, but it only considers the model of the outer DC-link voltage loop, whereas the inner current loop still utilize the conventional PI control strategy. The dynamic response and anti-disturbance performance of the inner current loop is not considered. Then they [23] proposed a DC-link voltage control strategy to ensure fast dynamic performance within its wide operation range. Instead of the conventional strategy with cascaded outer DC-link voltage loop and inner current loop, the proposed strategy is a direct voltage control strategy without an intermediate current loop.

H_∞ controller and μ controller with good robustness and simple structure could be adopted to improve capacity of resisting disturbance in the FESS, but their control performance relies heavily on accurate mathematical model of the FESS. Although other novel controllers based intelligent algorithm can also effectively tackle with self-adaptive problem, the high computation complexity goes against the improvement of dynamical response, and it increases the design cost of software and hardware beyond doubt. Therefore, it is hard for them to control dynamic performance of nonlinear systems in short time. However, the real-time dynamic control of DC-link voltage in discharge is significant in the FESS. Moreover, the dynamic equation of the DC-link voltage is a nonlinear function related to the motor rotational speed. If the control algorithm cannot properly tackle this nonlinear factor, the performance of system maybe deteriorated, even system may be unstable.

Fortunately, immersion and invariance manifold (I&IM) adaptive control strategy has many advantages for uncertain and nonlinear systems, such as having a simple structure, strong robustness, and extensive applications. Bai *et al*. [24] presented a function approximation technique based immersion and invariance control to address the problem in the nonlinear systems. Keighobadi *et al*. [25] used the I&IM to design an observer, whose problem is formulated as finding a dynamics system, and a differentiable manifold in the extended state space of the Euler angles-observer dynamics. Yi *et al*. [26] also designed state observers based on the I&IM for nonlinear systems. Thus, the I&IM adaptive control strategy plays a vital role and has practical value in the FESS. The I&IM adaptive control strategy uses two classical tools of nonlinear controller theory and of geometric nonlinear control systems, i.e., system immersion and manifold invariance, to reduce the problem of designing stable and adaptive control laws for general nonlinear systems [27]–[29]. The basic idea of the I&IM approach is to achieve the control objective by immersing the plant into a possibly low-order target system that captures the desired behavior. In adaptive control problems, the method yields stabilizing schemes that counter the effect of the uncertain parameters adopting a robustness perspective. In contrast with some of the existing adaptive controllers that treat these terms as disturbances to be rejected [30], the I&IM approach somehow is similar

to the procedure used in sliding mode control, where a given manifold, the sliding surface, is rendered attractive by a discontinuous control law [31]. The trajectories must reach the manifold in the sliding mode control, while in the I&IM approach the manifold needs not be reached, thus the high-frequency oscillation in the sliding-mode control is avoided. Indeed, there are other nonlinear controllers such as back-stepping controller and robust controller [32], [33], but these controllers' parameters need to be adjusted based on much experience, and these processes are time consuming.

Therefore, the I&IM adaptive control is chosen to realize the dynamic control of DC-link voltage in due course in that it only has three control parameters and less computation. The I&IM adaptive control not only can deal with control problems in the nonlinear controllers, but also can tackle self-adaptive problem of uncertainty which is a difficult problem for other nonlinear controllers. In particular, it is independent of the object model, is insensitive to the variation of system parameters, can restrain disturbance effectively, and can improve FESS robustness. Therefore, the I&IM is an effective method for solving the fluctuation problem of the DC-link voltage in the FESS.

The basic structure of the FESS controller is comprised of two loops. The inner one is current control loop, while the outer one is DC-link voltage control loop. Considering the nonlinear property of the DC-link voltage in discharge and the uncertain parameters in the PMSM/G based FESS, an affine nonlinear model is built involving the dynamic model of the inner current control loop in the system. Then the nonlinear controller is proposed using the I&IM approach, in which the instantaneous power of the load devices is regarded as a variable parameter. An adaptive law is also obtained via the I&IM approach. The stability of the overall system and the influence of the parameter error on the stability are verified by the Lyapunov stability theory, the influence of the parameter error on the transient characteristics of the closed-loop system is analyzed numerically. To investigate the performance of the proposed strategy, the I&IM controller of the DC-link voltage in the FESS in discharge is developed and realized on the experimental rig, and the experimental results in the whole available rotational speed range are obtained.

II. DYNAMIC CHARACTERISTICS OF THE DC-LINK VOLTAGE IN PMSM/G BASED FESS

Topology structure of FESS studied in this paper is shown in Fig. 1. The flywheel is coaxially connected with a PMSM/G, and driven by a bidirectional power converter. The DC bus capacitor acts as the interface to other parts of the system, which can be a source or a load, depending on the operational status.

Without considering non-linearity and hysteresis effect of iron corn in the PMSM/G, a simple model can be derived in the rotor flux orientation synchronous coordinates to

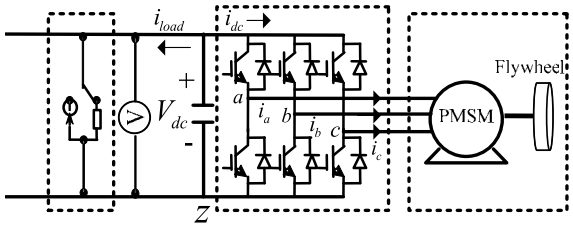

FIGURE 1. Topology structure of FESS.

represent the dynamic characteristics of the stator currents:

$$\begin{cases} v_{\mathrm{d}} = R_s i_d + L_s \dfrac{di_{\mathrm{d}}}{dt} - \omega L_{\mathrm{s}} i_{\mathrm{q}} \\ v_{\mathrm{q}} = R_{\mathrm{s}} i_{\mathrm{q}} + L_{\mathrm{s}} \dfrac{di_{\mathrm{q}}}{dt} + \omega L_{\mathrm{s}} i_{\mathrm{d}} + \omega \psi_{\mathrm{m}} \end{cases}, \tag{1}$$

where $i_{d,q}$ and $v_{d,q}$ are d-, q-axis stator current and voltage, respectively. R_s is the stator resistance, and L_s the stator inductance. ω is electrical angular velocity. ψ_m is the flux linkage of the PMSM/G.

According to the reference direction relation between the load current and the DC-link current shown in Fig. 1, dynamic equation of the DC-link voltage v_{dc} can be expressed as

$$C\frac{dv_{dc}}{dt} = -i_{dc} - i_{load}, \tag{2}$$

where C is the capacitor, i_{load} is the load current, i_{dc} and v_{dc} are the DC-link current and voltage, respectively.

When neglecting power loss of the converter, the power of the AC side equals that of the DC side, it is described as

$$v_{\mathrm{dc}} i_{\mathrm{dc}} = v_{az} i_a + v_{bz} i_b + v_{cz} i_c = \frac{3}{2}\left(v_{\mathrm{d}} i_{\mathrm{d}} + v_{\mathrm{q}} i_{\mathrm{q}}\right), \tag{3}$$

where v_{az}, v_{bz} and v_{cz} are the voltage drops from nodes a, b, and c to the node z, respectively, as illustrated in Fig. 1. i_a, i_b and i_c are the three-phase stator currents.

Substituting (1) and (3) into (2), the dynamic equation of the DC-link voltage in the PMSM/G based FESS will be

$$C\frac{dv_{\mathrm{dc}}^2}{dt} = -3\omega\psi_{\mathrm{m}} i_{\mathrm{q}} - 3R_{\mathrm{s}} i_{\mathrm{q}}^2 - 2P_{\mathrm{load}}, \tag{4}$$

in which $P_{load} = v_{dc} i_{load}$ is the load power. (3) and (4) are refer to [18] where describes the power balance between the PMSM/G and the bidirectional converter.

It is clear that (4) is a nonlinear system, so an appropriate nonlinear controller needs to be designed to meet the requirement of dynamic response in the FESS. Both sides of (4) are divided by C, and considering $dv_{dc}^2/dt = (v_{dc}^2 - v_{dc}^{*2})'$, it becomes

$$(v_{dc}^2 - v_{dc}^{*2})' = \frac{-3\omega\psi_m i_q}{C} - \frac{3R_s i_q^2}{C} - \frac{2P_{load}}{C}, \tag{5}$$

where v_{dc}^* is the reference value of the DC-link voltage. The current control loop of PMSM/G control system is assumed to be a first order inertia element, which is usually a practical choice. Owning to the FESS based on PMSM/G can be

regarded as a kind of PMSM control system, then concrete transfer function is described as

$$i_q(s)/i_q^*(s) = p_0/(s+p_0), \tag{6}$$

where i_q^* is the reference value of the q-axis current, p_0 represents the bandwidth of the inner current control loop.

Using the inverse Laplace transform, one can obtain the corresponding equation of (6) as

$$i_q' = p_0(i_q^* - i_q), \tag{7}$$

Further, combining (5) and (7) as

$$\begin{cases} (v_{dc}^2 - v_{dc}^{*2})' = \dfrac{-3\omega\psi_m i_q}{C} - \dfrac{3R_s i_q^2}{C} - \dfrac{2P_{load}}{C} \\ i_q' = -p_0 i_q + p_0 i_q^* \end{cases}. \tag{8}$$

Subsequently, (8) is transferred into matrix form as

$$\begin{aligned} \begin{bmatrix} (v_{dc}^2 - v_{dc}^{*2})' \\ i_q' \end{bmatrix} &= \begin{bmatrix} 0 & -3\omega\psi_m i_q/C \\ 0 & -p_0 \end{bmatrix} \begin{bmatrix} v_{dc}^2 - v_{dc}^{*2} \\ i_q \end{bmatrix} \\ &\quad - \begin{bmatrix} 0 & -3R_s/C \\ 0 & 0 \end{bmatrix} \begin{bmatrix} (v_{dc}^2 - v_{dc}^{*2})^2 \\ i_q^2 \end{bmatrix} \\ &\quad - \begin{bmatrix} 2P_{load}/C \\ 0 \end{bmatrix} + \begin{bmatrix} 0 \\ p_0 \end{bmatrix} i_q^*. \end{aligned} \tag{9}$$

Equation (9) is a second-order nonlinear system with the state variables $x = (x_1, x_2)^{\mathrm{T}}$, in which $x_1 = v_{dc}^2 - v_{dc}^{*2}$, $x_2 = i_q^*$, i_q^* is seen as the control input. Then the state equation of DC-link voltage in the FESS is

$$\begin{aligned} \begin{bmatrix} \dot{x}_1 \\ \dot{x}_2 \end{bmatrix} &= \begin{bmatrix} 0 & -3\omega\psi_m i_q/C \\ 0 & -p_0 \end{bmatrix} \begin{bmatrix} x_1 \\ x_2 \end{bmatrix} - \begin{bmatrix} 0 & -3R_s/C \\ 0 & 0 \end{bmatrix} \begin{bmatrix} x_1^2 \\ x_2^2 \end{bmatrix} \\ &\quad - \begin{bmatrix} 2P_{load}/C \\ 0 \end{bmatrix} + \begin{bmatrix} 0 \\ p_0 \end{bmatrix} u. \end{aligned} \tag{10}$$

However, considering the dynamic characteristics of the inner current loop in the model, (10) can be transformed to an affine nonlinear system, i. e.,

$$\begin{cases} \dot{x}_1 = ax_2 - bx_2^2 - \theta \\ \dot{x}_2 = -p_0 x_2 + p_0 u \end{cases} \tag{11}$$

where $x_1 = v_{dc}^2 - v_{dc}^{*2}$, $x_2 = i_q^*$, $a = -3\omega\psi_m/C$, $b = 3\,R_s/C$, $\theta = 2\,P_{load}/C$.

III. IMMERSION AND INVARIANCE MANIFOLD ADAPTIVE CONTROLLER DESIGN

A. THE I&IM STABILIZATION THEORY

Remark 1. The I&IM adaptive control strategy plays a vital role and has practical value in the FESS. The I&IM adaptive control strategy uses two classical tools of nonlinear controller theory and of geometric nonlinear control systems, i.e., system immersion and manifold invariance, to reduce the problem of designing stable and adaptive control laws for general nonlinear systems [8], [20], [21].

The basic result for the I&IM stabilization theory includes a set of sufficient conditions for the construction of globally asymptotically stabilizing static state feedback control law for affine nonlinear systems.

Consider the system

$$\dot{x} = f(x) + g(x)u \tag{12}$$

with $x \in \mathbb{R}^n$, $u \in \mathbb{R}^m$, and an equilibrium $x^* \in \mathbb{R}^n$ to be stabilized. Assume that there exist smooth mappings α: $\mathbb{R}^p \to \mathbb{R}^p$, π: $\mathbb{R}^p \to \mathbb{R}^n$, ϕ: $\mathbb{R}^n \to R^{(n-p)}$, c: $\mathbb{R}^p \to \mathbb{R}^m$, v: $\mathbb{R}^{n\times(n-p)} \to \mathbb{R}^m$, with $p < n$, such that the following results hold.

(A1) The target system

$$\dot{\xi} = \alpha(\xi), \tag{13}$$

with $\xi \in \mathbb{R}^p$ has a globally asymptotically stable equilibrium at $\xi^* \in \mathbb{R}^p$ and $x^* = \pi(\xi^*)$.

(A2) For all $\xi \in \mathbb{R}^p$,

$$f[\pi(\xi)] + g[\pi(\xi)]c[\pi(\xi)] = \frac{\partial \pi}{\partial \xi}\alpha(\xi). \tag{14}$$

(A3) The set identity holds

$$M = \{x \in R^n | \phi(x) = 0\} = \{x \in R^n | x = \pi(\xi), \xi \in R^p\} \tag{15}$$

(A4) The manifold attractivity and trajectory boundedness are designed as

$$\dot{z} = \frac{\partial \phi}{\partial x}[f(x) + g(x)v(x,z)], \tag{16}$$

$$\dot{x} = f(x) + g(x)v(x,z), \tag{17}$$

with the initial condition constraint

$$z(0) = \phi[x(0)], \tag{18}$$

and $v(x,z)$ verifying

$$v[\pi(\xi), 0] = c[\pi(\xi)], \forall \xi \in R^p. \tag{19}$$

All trajectories of the system are bounded and satisfy

$$\lim_{t\to\infty} z(t) = 0. \tag{20}$$

Then x^* is a globally asymptotically stable equilibrium of the closed-loop system

$$\dot{x} = f(x) + g(x)v[x, \phi(x)]. \tag{21}$$

The procedure of I&IM stabilization theory's derivation is: Choose the target system (16) to obtain the manifold M, then design the control input $v[x, \phi(x)]$ to make M invariance and asymptotically stable, therefore the system will converge to the equilibrium point x^* asymptotically.

B. THE I&IM ADAPTIVE CONTROLLER DESIGN

Remark 2. There are other nonlinear controllers such as back-stepping controller and robust controller [24], [25], but these controllers' parameters need to be adjusted based on much experience, and these processes are time consuming. Therefore, the I&IM is an effective method for solving the fluctuation problem of the DC-link voltage in the FESS.

Specify the desired dynamic characteristic of the system as

$$\dot{\xi} = -\lambda_1 \xi, \tag{22}$$

where $\lambda_1 > 0$ is the parameter to adjust the dynamic performance of the system.

It is clear that (22) has a globally asymptotical stable equilibrium point at $\xi^* = 0$. Then using (11) and (17), we can derive $\dot{x}_1 - ax_2 - bx_2^2 - \theta = 0$ with $\dot{x}_1 = -\lambda_1 x_1$, (15) shows $\phi(x) = 0$, it means $\dot{x}_1 - ax_2 - bx_2^2 - \theta = \phi(x)$. We let the mapping relationship be $x_1 = \xi$, so the manifold is derived as

$$\phi(x) = ax_2 - bx_2^2 - \theta + \lambda_1 x_1. \tag{23}$$

According to the discussion above, once $\phi(x) = 0$ is satisfied, the convergence rule $\dot{x}_1 = -\lambda_1 x_1$ is obtained, and subsequently, the state variable of the system will asymptotically converge to the equilibrium $x_1^* = 0$.

Equation (23) is derived to obtain

$$\dot{\phi} = (a - 2bx_2)[-p_0 x_2 + p_0 v(x, \phi)] + \lambda_1(ax_2 - bx_2^2 - \theta). \tag{24}$$

If the control input is chosen as

$$v(x, \phi) = \frac{-(\lambda_1 + \lambda_2)\phi + \lambda_1^2 x_1}{p_0(a - 2bx_2)} + x_2, \tag{25}$$

then we have $\dot{\phi} = -\lambda_2 \phi$, and $\phi^* = 0$ is a globally asymptotically stable equilibrium point.

The variable parameter θ in the system is determined by the instantaneous load power P_{load}, thus its value is unknown. In cases when the load devices are power electronic pieces of equipment, the load current is different according to the state of the power switches, so P_{load} cannot be detected in real-time by measuring the load current. Thus, we have to design an adaptive law to estimate the value of θ. Using the I&IM approach, the estimated value $\hat{\theta}$ can be expressed as

$$\hat{\theta} = \theta_I + \theta_P(x), \tag{26}$$

where θ_I is the integral term, and θ_P is the proportional term.

Set the estimation error to be $z = \hat{\theta} - \theta$, then its derivative is

$$\dot{z} = \dot{\theta}_I + \frac{\partial \theta_P}{\partial x_1}(ax_2 - bx_2^2 - (\hat{\theta} - z)) + \frac{\partial \theta_P}{\partial x_2}(-p_0 x_2 + p_0 u). \tag{27}$$

If the term $\dot{\theta}_I$ is assigned to be

$$\dot{\theta}_I = -\frac{\partial \theta_P}{\partial x_1}(ax_2 - bx_2^2 - \hat{\theta}) - \frac{\partial \theta_P}{\partial x_2}(-p_0 x_2 + p_0 u), \tag{28}$$

then (27) can be simplified as

$$\dot{z} = \frac{\partial \theta_P}{\partial x_1} z. \tag{29}$$

If, further, choosing the value of θ_P as

$$\theta_P = -\lambda_3 x_1, \tag{30}$$

then it can be obtained that $\dot{z} = -\lambda_3 z$, the equilibrium point $z^* = 0$ is asymptotically stable.

Substituting (30) into (28), the expression of $\dot{\theta}_I$ is derived as

$$\dot{\theta}_I = \lambda_3(ax_2 - bx_2^2 - \hat{\theta}). \tag{31}$$

If the variable parameter θ is replaced by $\hat{\theta}$, $\phi(x)$ becomes

$$\phi(x) = ax_2 - bx_2^2 - \hat{\theta} + z + \lambda_1 x_1 = \tilde{\phi}(x) + \lambda_1 x_1. \tag{32}$$

where $\tilde{\phi}(x) = ax_2 - bx_2^2 - \hat{\theta} + z$.

Subsequently, the extended system with the state variables (ϕ, z, x_1, x_2) can be obtained by substituting (32) and (25) into (11). The dynamic equations are

$$\begin{cases} \dot{\phi}(x) = -\lambda_2 \phi + (\lambda_1 + \lambda_3) z \\ \dot{z} = -\lambda_3 z \\ \dot{x}_1 = -\lambda_1 x_1 + \phi + z \\ \dot{x}_2 = \frac{-(\lambda_1 + \lambda_2)\phi + \lambda_1^2 x_1}{a - 2bx_2} \end{cases}. \tag{33}$$

For the subsystem of (33) with the state variables (ϕ, z, x_1), it is clear that its equilibrium point is at the origin (0, 0, 0). Consider now the Lyapunov function $V_a = (\phi + x_1^2 + k_1 z^2)/2$, whose time-derivative along the trajectories of (33) is

$$\begin{aligned} \dot{V}_a = &-\frac{1}{2}(\lambda_1 x_1^2 + \lambda_2 \phi^2 - 2x_1 \phi) - \frac{1}{2}(\lambda_1 x_1^2 + k_1 \lambda_3 z^2 - 2x_1 z) \\ &-\frac{1}{2}[\lambda_2 \phi^2 + k_1 \lambda_3 z^2 - 2(\lambda_1 + \lambda_3)\phi z], \end{aligned} \tag{34}$$

where $k_1 > 0$ is a coefficient to be determined.

Using the inequality analysis technique, $\dot{V}_a \leq 0$ can be satisfied when

$$\sqrt{\lambda_1 \lambda_2} \geq 1, \sqrt{k_1 \lambda_1 \lambda_3} \geq 1, \sqrt{k_1 \lambda_2 \lambda_3} \geq \lambda_1 + \lambda_3. \tag{35}$$

Obviously, the inequalities hold if k_1 is big enough. As a consequence, the subsystem with the state variables (ϕ, z, x_1) is globally asymptotically stable at the equilibrium (0, 0, 0), while x_2 will converge to the corresponding value and vary according to the instantaneous load power P_{load}.

C. THE CONVERGENCE ANALYSIS OF I&IM ADAPTIVE CONTROLLER

It is known from the above discussion that the stability of the I&IM adaptive controller is verified via the Lyapunov stability theory, but we hardly obtain the convergence characteristics of the stator current from theory. The convergence characteristics of the stator current are greatly depended on the parameters λ_1, λ_2 and λ_3 of the I&IM adaptive controller. According to (22), λ_1 represents state variable x_1, the control accuracy of the FESS is dependent on it. Due to the existence of equilibrium point based on the transfer function characteristics of closed loop system, then $\lambda_1 > 0$. λ_2 represents auxiliary state ϕ which has a great influence on the rapidity of globally asymptotical stability. λ_3 stands for the convergence rate of adaptive parameter error z, which can guarantee that the FESS achieves stable state in finite time. The value of λ_3 is limited by (35) to satisfy Lyapunov stability theory.

Therefore, the effects of the parameters λ_1, λ_2 and λ_3 on the system transient characteristics have to be investigated to get a perception of the controller design.

When the stator resistance is ignore, i.e., let $b = 0$ in the system model (11), linear approximation system is derived as

$$\begin{cases} \dot{x}_1 = ax_2 - \theta \\ \dot{x}_2 = -p_0 x_2 + p_0 u \end{cases}. \tag{36}$$

Using the I&IM approach, the control law for (36) can be summarized as

$$\begin{cases} \theta_P = -\lambda_3 x_1 \\ \dot{\theta}_I = \lambda_3(ax_2 - \theta_I - \theta_P) \\ \phi(x) = ax_2 - \theta_I - \theta_P + \lambda_1 x_1 \\ u = \dfrac{-(\lambda_1+\lambda_2)\phi + \lambda_1^2 x_1}{p_0 a} + x_2 \end{cases}. \tag{37}$$

Substituting (37) into (36), the resulted closed-loop system can be derived and expressed in the form of transfer function from θ to x_1 and θ to x_2 as

$$\frac{x_1(s)}{\theta(s)} = \frac{-s(s+\lambda_1+\lambda_2+\lambda_3)}{(s+\lambda_1)(s+\lambda_2)(s+\lambda_3)}, \tag{38}$$

$$\frac{x_2(s)}{\theta(s)} = \frac{(\lambda_1\lambda_2+\lambda_2\lambda_3+\lambda_1\lambda_3)s + \lambda_1\lambda_2\lambda_3}{a(s+\lambda_1)(s+\lambda_2)(s+\lambda_3)}. \tag{39}$$

It can be seen that both the transfer functions from θ to x_1 and θ to x_2 are three-order, the steady state value of x_1 is 0, and that of x_2 is θ/a. The parameters λ_1, λ_2 and λ_3 are three poles of the closed-loop system, and as a result, they determine its transient characteristics.

The inevitable modeling error of the system will make the experimental results deviate from the theoretical prediction. Thus the controller parameters have to be adjusted according to the actual situation. A theorem is achieved:

Theorem 1: Although these three parameters in the controller represent symmetrical relationship in (38) and (39), while according to the inequalities shown in (35) and the experimental debugging results, choosing $\lambda_2 > \lambda_3 > \lambda_1$ will result in better system performance.

This Theorem is also verified sufficiently in simulations and experiments.

D. THE EFFECTIVENESS OF THE I&IM ADAPTIVE CONTROLLER

The I&IM adaptive controller can make the state variable x_1 converge to the origin asymptotically, i.e., keep the DC-link voltage of FESS discharge constant at the desired level when load power varies.

To gain intuition on the performance of the I&IM adaptive controller, numerical simulations are taken to investigate the tracking performance of the estimated value $\hat{\theta}$ and state variable with the I&IM adaptive controller. Set the load power P_{load} to be a typical step 1kW →2kW →–2kW. According to the current limit of the experimental rig, the limit of the control input is set as $-15 \le u \le 15$. The simulation results are shown in Fig. 2.

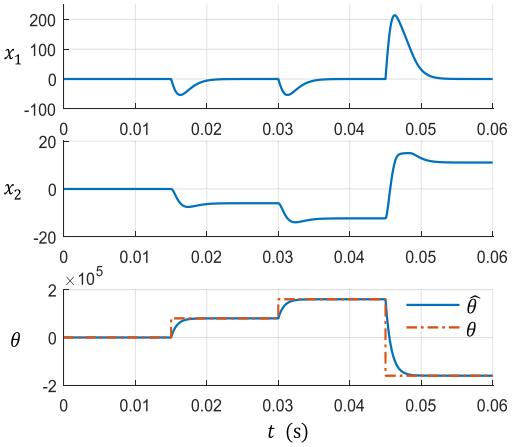

FIGURE 2. Simulation of the system states and parameter estimation.

It is clearly shown that the state variable x_1 converges to 0 asymptotically regardless of the variation of P_{load}, and x_2 converges to the corresponding equilibrium value. It means that the value of v_{dc}^* equals that of v_{dc}, and i_q is a constant. The estimated parameter $\hat{\theta}$ tracks the real value θ well, and its transient performance has the characteristics of a first-order system, as assigned in (31).

IV. EFFECTS OF THE PARAMETER DEVIATION ON SYSTEM PERFORMANCE

In most cases, it is almost impossible to get the actual parameter value in practical applications, for the parameters always drift according to the operating conditions. Therefore, it is necessary to evaluate the effects of parameter error on the system performance with the I&IM adaptive controller. In this section, we take the influence of the stator resistance error to investigate the level of these effects as an example.

Represent the nominal parameter used in the controller as $\hat{b} = b + \Delta b$, where Δb is a parameter error. Then the expression of $\phi(x)$ becomes

$$\phi(x) = ax_2 - (b+\Delta b)x_2^2 - \hat{\theta} + \lambda_1 x_1. \tag{40}$$

Substituting (40) into the controller expression, the system of the extended state variables (ϕ, z, x_1, x_2) with the parameter error Δb can be derived as

$$\begin{cases} \dot{\phi}(x) = -\lambda_2\phi + (\lambda_1+\lambda_3)(z + \Delta b x_2^2) \\ \dot{z} = -\lambda_3(z + \Delta b x_2^2) \\ \dot{x}_1 = -\lambda_1 x_1 + \Delta b x_2^2 + \phi + z \\ \dot{x}_2 = \dfrac{-(\lambda_1+\lambda_2)\phi + \lambda_1^2 x_1}{a - 2(b+\Delta b)x_2} \end{cases} \tag{41}$$

The equilibrium point of the system (41) is at $(0, -\Delta b(x_2^*)^2, 0, x_2^*)$, thus Δb only deviates the equilibrium point of z from 0 and did not affect the equilibrium point of ϕ and x_1. To investigate the system stability when Δb exists, we adopt an auxiliary variable $z_1 = z + \Delta b x_2^2$, then system is

expressed as

$$\begin{cases} \dot{\phi}(\xi) = -\lambda_2\phi + (\lambda_1+\lambda_3)z_1 \\ \dot{z} = -\lambda_3 z_1 + 2\Delta b x_2^2 \dfrac{-(\lambda_1+\lambda_2)\phi + \lambda_1^2 x_1}{a-2(b+\Delta b)x_2} \\ \dot{x}_1 = -\lambda_1 x_1 + \phi + z_1 \\ \dot{x}_2 = \dfrac{-(\lambda_1+\lambda_2)\phi + \lambda_1^2 x_1}{a-2(b+\Delta b)x_2} \end{cases} \tag{42}$$

Considering the Lyapunov function $V_b = (\phi + x_1^2 + k_1 z_1^2)/2$, the time-derivative of V_b along the trajectories of (42) is

$$\begin{aligned} \dot{V}_b = & \frac{1}{2}(\lambda_1 x_1^2 + \lambda_2\phi^2 - 2x_1\phi) \\ & -\frac{1}{2}[\lambda_1 x_1^2 + k_1\lambda_3 z_1^2 - 2(1+k_1\lambda_1^2\sigma)x_1 z_1] \\ & -\frac{1}{2}\{\lambda_2\phi^2 + k_1\lambda_3 z_1^2 - 2[\lambda_1+\lambda_3 - k(\lambda_1+\lambda_2)\sigma]\phi z_1\} \end{aligned} \tag{43}$$

where $\sigma = \frac{2\Delta b x_2}{a-2(b+\Delta b)x_2}$.

When the equilibrium point of the state variables (ϕ, z_1, x_1) in (42) is at (0, 0, 0). $\dot{V}_b \le 0$ is satisfied when

$$\begin{aligned} \sqrt{\lambda_1\lambda_2} &\ge 1 \\ \sqrt{k_1\lambda_1\lambda_3} &\ge 1 + k_1\lambda_1^2\sigma \\ \sqrt{k_1\lambda_2\lambda_3} &\ge \lambda_1 + \lambda_3 - k_1(\lambda_1+\lambda_2)\sigma. \end{aligned} \tag{44}$$

Consider now the physical meaning of these parameters, $\omega\psi_m$ is the back electromotive force in the stator winding, $R_s i_q$ is the voltage of the stator resistance, therefore we have

$$\frac{a}{bx_2} = -\frac{\omega\psi_m}{R_s i_q}. \tag{45}$$

Since the magnitude of the back electromotive force is often larger than the voltage of the stator resistance, the range of $|\sigma|$ is limited within $0< |\sigma| <1$. As a matter of fact, (44) can be regarded as a set of constraints for λ_1, λ_2 and λ_3. When these inequalities are satisfied, the closed-loop system is stable and the state variables (ϕ, z_1, x_1) will asymptotically converge to the equilibrium point (0, 0, 0).

Since the resistance of the motor winding R_s varies with the motor's temperature in the actual system, so R_s is a main parameter to cause modeling error in the process of controller design. Therefore, we take the influence of the stator resistance error to investigate the level of these effects as an example. Besides, considering the effect of magnetic saturation, the deviation of flux linkage ψ_m was also been discussed. According to (23) and (11), considering $\hat{a} = a + \Delta a$, wher $\hat{a}$ and Δa represent the nominal parameter and deviation caused by flux linkage ψ_m, respectively, then the expression of ϕ becomes

$$\phi = (a+\Delta a)x_2 - bx_2^2 - \theta - z + \lambda_1 x_1. \tag{46}$$

Considering (11) and (25), $\dot{x}_2$ can be expressed as

$$\dot{x}_2 = -p_0 x_2 + p_0 u = -[(\lambda_1+\lambda_2)\phi + \lambda_1^2 x_1]/(a+2bx_2) \tag{47}$$

In order to analyze the effect of Δa on the system stability, we adopt an auxiliary variable $z_2 = z + \Delta a x_2$ and substitute (46) into the controller expression, then the system can be derived as

$$\begin{cases} \dot{\phi}(x) = -\lambda_2\phi + (\lambda_1+\lambda_3)(z+ax_2) \\ \dot{z}_2 = \dot{z} + \Delta a\dot{x}_2 = -\lambda_3 z_2 + \dot{x}_2 \\ \dot{x}_1 = \phi - \lambda_1 x_1 + z_2 - 2\Delta a x_2 \\ \dot{x}_2 = \dfrac{-(\lambda_1+\lambda_2)\phi + \lambda_1^2 x_1}{a+\Delta a - 2bx_2} \end{cases} \tag{48}$$

Choosing candidate Lyapunov function $V_c = (\phi + x_1^2 + k_1 z_2^2)$, and the time-derivative of V_b along the trajectories of (48) is

$$\begin{aligned} \dot{V}_b &= (\dot{\phi} + 2x_1\dot{x}_1 + 2k_1 z_2\dot{z}_2) \\ &= -\lambda_2\phi + (\lambda_1+\lambda_3)z_2 + 2x_1(-\lambda_1 x_1 + \phi \\ &\quad + z_2 - 2\Delta a x_2) + 2k_1 z_2[-\lambda_3 z_2 + \sigma_1(\lambda_1+\lambda_2)\phi + \lambda_1^2 x_1] \\ &= -(\lambda_1 x_1^2 + \lambda_2\phi^2 - 2x_1\phi) - [\lambda_1 x_1^2 + k_1\lambda_3 z_2^2 \\ &\quad + 2(1+k_1\lambda_1^2\sigma_1)x_1 z_2] \\ &\quad - \{\lambda_2\phi^2 + k_1\lambda_3 z_2^2 - 2[\lambda_1+\lambda_3 \\ &\quad - k_1(\lambda_1+\lambda_2)\sigma_1]\phi z_1\} - 4x_1\Delta a x_2 \end{aligned} \tag{49}$$

where $\sigma_1 = \Delta a/[(a+\Delta a) - 2bx_2]$.

The following steps are to ensure the candidate Lyapunov function $V_c = (\phi + x_1^2 + k_1 z_2^2)$ is non-negative:

Step1: In $V_c = (\phi + x_1^2 + k_1 z_2^2)$, if $\varphi \ge 0$, then $V_c = (\phi + x_1^2 + k_1 z_2^2) \ge 0$, where $k_1 > 0$. Therefore, we should verify φ is non-negative;

Step2: In (23), $\phi(x) = ax_2 - bx_2^2 - \theta + \lambda_1 x_1$. In (11), $\dot{x}_1 = ax_2 - bx_2^2 - \theta$, then $\phi(x) = \dot{x}_1 + \lambda_1 x_1$;

Step3: According to (22), we make $\dot{x}_1 = -\lambda_1 x_1$, therefore $\phi(x) = 0$;

Step4: The candidate Lyapunov function $V_c = (\phi + x_1^2 + k_1 z_2^2)$ is non-negative.

When the equilibrium point of the state variables (ϕ, z_2, x_1) in (49) is at (0, 0, 0). $\dot{V}_c \le 0$ is satisfied when

$$\begin{aligned} &\sqrt{\lambda_1\lambda_2} \ge 1, \sqrt{k_1\lambda_1\lambda_3} \ge 1 + k_1\lambda_1^2\sigma_1, \Delta a x_1 x_2 \le 0, \\ &\sqrt{k_1\lambda_2\lambda_3} \ge \lambda_1 + \lambda_3 - k_1(\lambda_1+\lambda_2)\sigma_1. \end{aligned} \tag{50}$$

Since deviations of coefficient a and b are indpendent of the inductance, so the inductance cannot have a direct effect on performance of the controller. In order to analyze the effect of both Δa and Δb on the system stability, the auxiliary variable $z_3 = z + \Delta a x_2 + \Delta b x_2^2$ is adopted. The concrete derivation processes are similar to single parameter deviation such as (42) and (48).

The numerical simulation results in cases of $\Delta b = \pm 0.5b$ are shown in Fig. 3 with different deviations. As a comparison with the case when $\Delta b = 0$, the parameters of the model and the controller are similar to those in Fig. 2. It is shown that the estimated parameter $\hat{\theta}$ will converge to different values according to variation of Δb, but x_1 will always converge to 0, and the differences of the transient performance between these three cases are rather small.

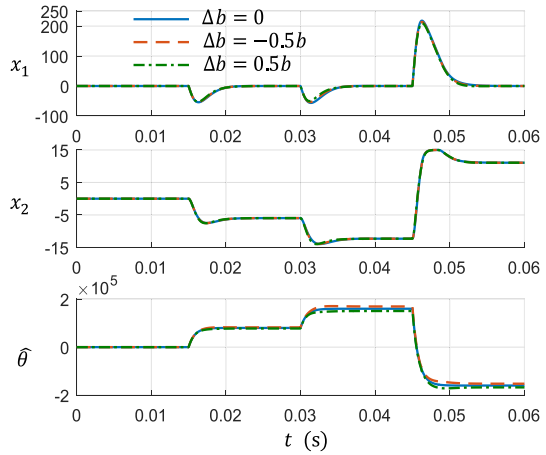

FIGURE 3. Simulation of the system states and parameter estimation when Δb exists.

Theorem 2: The parameter error in the system model hardly affects the steady value of the DC-link voltage, and has a small impact on the transient performance of the system.

V. SIMULATION AND EXPERIMENT RESULTS

In order to validate the proposed I&IM adaptive control algorithm for the wide rotational speed range in the FESS discharge, the simulation and experiment were conducted and the results are presented in this section.

A. SIMULATION RESULTS OF THE FESS DISCHARGE OVER THE WIDE ROTATIONAL SPEED RANGE

A simulation model for the FESS was built in the electrical engineering software PLECS, the PLECS is the tool of choice for high-speed simulations of power electronic systems, it is available for seamless integration with MATLAB/Simulink. The block diagram is shown in Fig. 4. The hardware structure of this model is composed of a PMSM/G, a three-phase converter, a capacitor for energy storage and a load resistance. The parameters of the FESS used in the simulations are similar to those of the prototype experimental rig, which are shown in Table 1.

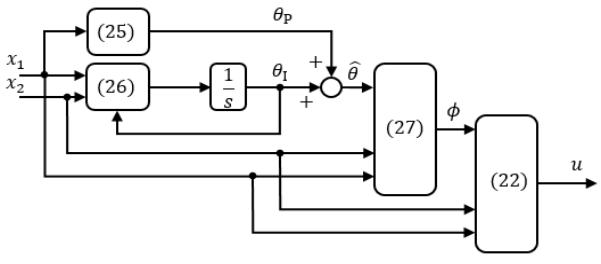

FIGURE 4. Block diagram of the FESS for simulation.

The controller of the system includes a DC-link voltage controller, an inner current controller and a space vector pulse-width modulation (SVPWM) module. The DC-link voltage controller takes the error between the reference value v_{dc}^* and the measured value v_{dc} as the input, and outputs the reference current i_q^* to the inner current controller. The reference stator voltages, v_d and v_q, then can be obtained from the current controller. They will be converted to pulse sequences to drive the converter via the SVPWM module.

TABLE 1. Parameters of the PMSM/G experimental rig.

Parameter	Value
Stator Inductance	3.521 mH
Stator Resistance	0.171 Ω
Permanent Magnet Flux Linkage	0.0913 Wb
Maximal Speed	12000 r/min
Rated Stator Current	15 A
Rotor Moment of Inertia	7 g·m^2
Pole Pairs of PMSM/G	1
DC-link Capacitor	21.2 mF
Rated DC-link Voltage	300 V
Sampling Frequency	10 kHz

When the parameters of the I&IM adaptive controller are $\lambda_1 = \lambda_2 = \lambda_3 = 200\pi$, the simulation results of the FESS in discharge process are shown in Fig. 5(a), in which the load power P_{load} is set as a step voltage sequence 0 kW→2 kW→0 kW. The corresponding rotational speed at the step time is 11500 r/min. It is shown that the DC-link voltage v_{dc} can achieve steady state immediately as soon as the load power steps, the recovery time is smaller than 0.2 s and the peak value of the voltage fluctuations is smaller than 5 V. Moreover, the stator current i_q converges to a value to follow the load variety, and $\hat{\theta}$ tracks changes of the load power P_{load} smoothly. When $\lambda_1 = \lambda_2 = \lambda_3 = 1000\pi$, the simulation results of the FESS in discharge process are shown in Fig. 5 (b). Compared with Fig. 5 (a), Fig. 5 (b) shows that the dynamic response performance is improved to shorten transient process by increasing the parameters values of the I&IM adaptive controller from 200π to 1000π. $\hat{\theta}$ and i_q still keep convergence smooth, the recovery time and peak value of the DC-link voltage decrease to 0.05 s and 1 V in the case of the $\lambda_1 = \lambda_2 = \lambda_3 = 1000\pi$, respectively. During the discharge process of the FESS, the rotational speeds drop and i_a varies to follow the load variety accordingly.

Besides, based on the theoretical analysis and parameter selection principle of section *C* of chapter III, the parameters of the I&IM adaptive controller need to meet the numerical relationship $\lambda_2 > \lambda_3 > \lambda_1$ to improve the transient characteristics to a large extent. In order to make (50) hold, λ_1, λ_2, and λ_3 should be chosen reasonably. If λ_1, λ_2, and λ_3 satisfy (50), then $\dot{V}_c \leq 0$. The control performance varies with the parameters λ_1, λ_2, and λ_3. The simulation results of the FESS in discharge process in the case of the $\lambda_1 = 10\pi$, $\lambda_2 = 240\pi$, $\lambda_3 = 40\pi$ are shown in Fig. 6, in which the load power P_{load} is set as a step voltage sequence 0 kW→2 kW→1.5 kW→0.6 kW→0 kW. The corresponding rotational speeds at the step time are 12000, 10000,

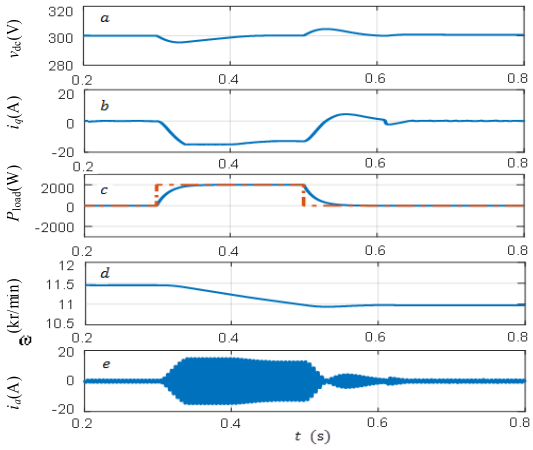

(a)

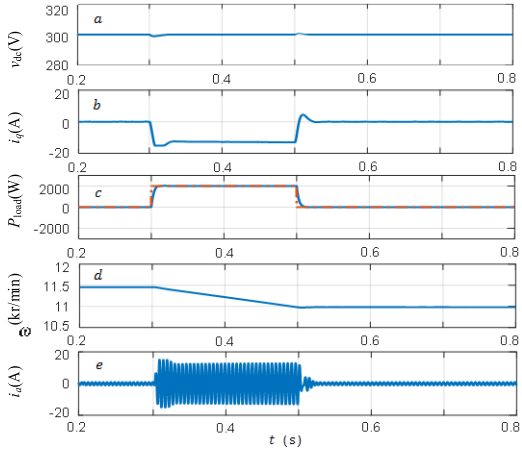

(b)

FIGURE 5. Discharge process of FESS. (a) $\lambda_1 = \lambda_2 = \lambda_3 = 200\pi$. (b) $\lambda_1 = \lambda_2 = \lambda_3 = 1000\pi$.

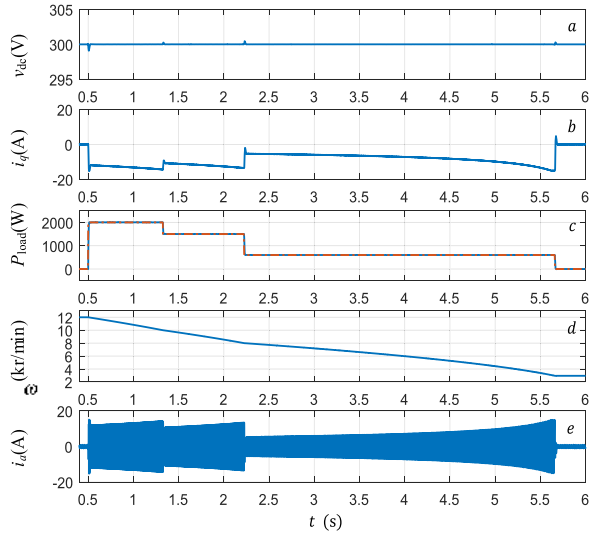

FIGURE 6. Discharge process of the FESS, in which the parameters of the I&IM adaptive controller are $\lambda 1 = 10\pi$, $\lambda 2 = 240\pi$, $\lambda 3 = 40\pi$.

8000 and 3000 r/min, respectively. It is shown that the stator current i_q changes immediately as soon as the load

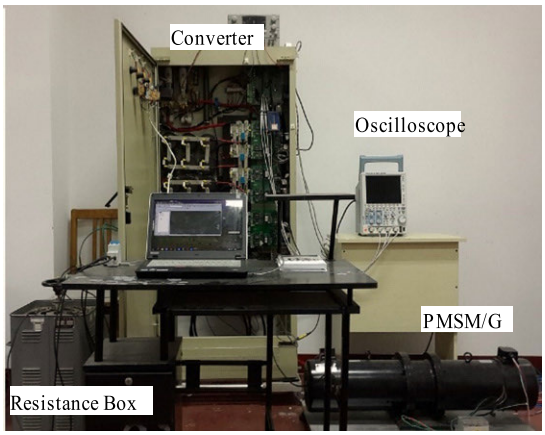

FIGURE 7. PMSM/G prototype experimental rig.

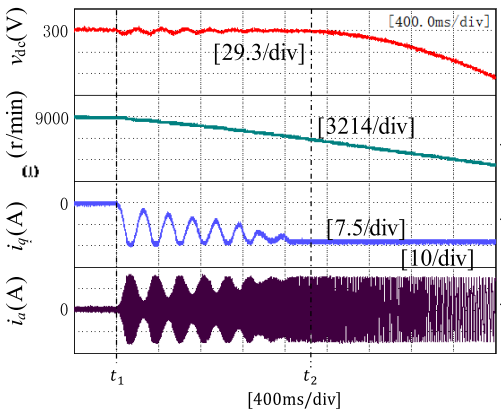

(a)

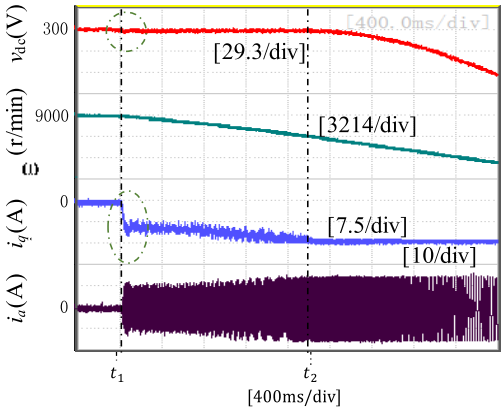

(b)

FIGURE 8. Experimental discharge waveforms of the I&IM adaptive controller. (a)$\lambda 1 = \lambda 2 = \lambda 3 = 400\pi$. (b) $\lambda 1 = 10\pi$, $\lambda 2 = 240\pi$, $\lambda 3 = 40\pi$.

power changes. The transient process is short and the current waveform is smooth, thus the voltage fluctuations of v_{dc} at the four step points are very small. The favorable results hold in the wide rotational speed range, and the peak value of the voltage fluctuations is smaller than 1 V.

As the rotational speed decreases from 12000 to 3000 r/min, the DC-link voltage is kept stable at the reference

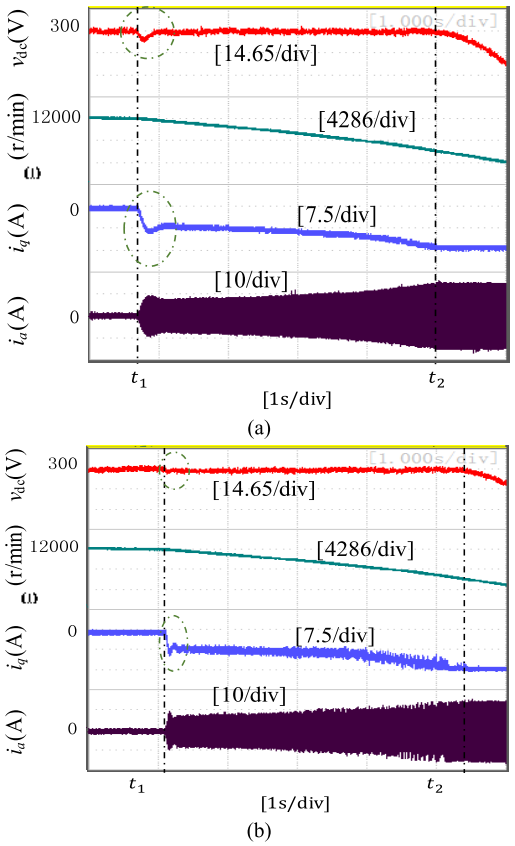

FIGURE 9. Experimental discharge waveforms with the initial speed of 12000 r/min, the impact load of 120Ω. (a) PI controller. (b) I&IM adaptive controller.

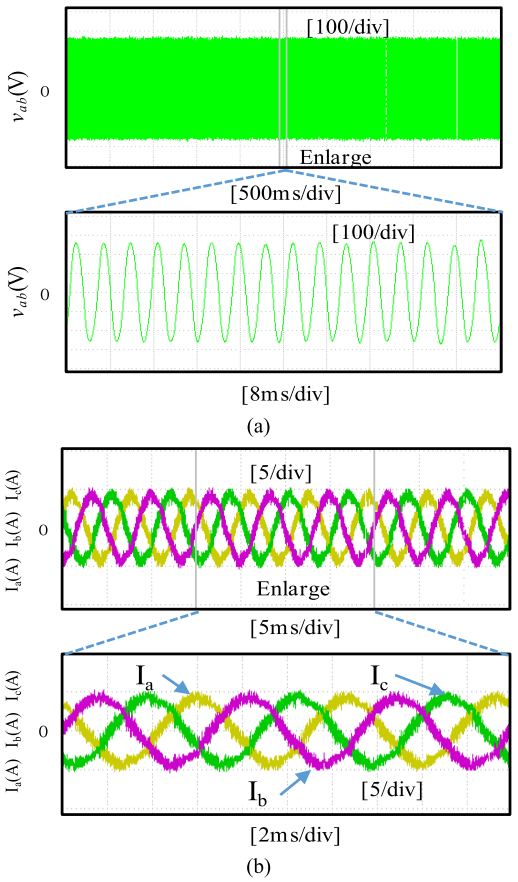

FIGURE 10. Experimental waveforms of line voltage and line current of PMSM/G with 12000 r/min. (a) line voltage. (b) line current.

value 300 V in spite of the change of load power. It can be concluded that the proposed I&IM adaptive controller can maintain good characteristics during wide rotational speed range operation.

B. EXPERIMENTAL PERFORMANCE BETWEEN THE I&IM ADAPTIVE CONTROLLER AND THE PI CONTROLLER OVER WIDE ROTATIONAL SPEED RANGE

In order to compare the system performances between the proposed I&IM adaptive controller and the traditional PI controller over a wide rotational speed range, the experiments were carried out on the FESS prototype experimental rig shown in Fig. 7. The experimental rig is consisted of a PMSM/G, a converter, a coaxially connected induction motor and a resistance box, which can be used to imitate the operation of a FESS. The resistance box acts as the load of the system here. In the experiment, same gains for the PI controller are used at different ranges. These gains have been adjusted to the optimal ones to achieve satisfactory control performance, where proportional gain k_p and integrating gain k_i are 0.6 and 10, respectively.

The discharge process of the FESS was realized in the prototype experimental rig at three typical initial rotational speeds of 12000, 9000 and 6000 r/min, respectively. At first, the PMSM was accelerated to the desired initial rotational speed by a coaxially connected induction motor, which was driven by a commercial converter. Then the converter was disconnected, and the intial DC-link voltage was stabilized at 300 V in non-loaded condition. After that, a transient loading test was conducted for both the two control methods to compare the dynamic performance. The overall control structure of the experimental rig is similar to the simulation model.

Before the contrast experiment between the PI controller and I&IM adaptive controller, the convergence characteristics of the stator current with $\lambda_2 > \lambda_3 > \lambda_1$ are verified in advance. The parameters of the PI controller are chosen as optimal ones obtained in experiments. The experimental results with the initial rotational speed of 9000 r/min are shown in Fig. 8. It was observed that if the parameters in the I&IM adaptive controller are equal, e.g., the experimental results of $\lambda_1 = \lambda_2 = \lambda_3 = 400\pi$ as show in Fig. 8(a), the oscillation appears in the waveform of i_q during the convergence, whereas convergence is fast when $\lambda_1 = 10\pi$, $\lambda_2 = 240\pi$ and $\lambda_3 = 40\pi$ in Fig. 8(b).

The DC-link voltage waveforms in the transient loading discharge test with the initial rotational speed of 12000 r/min and the impact load of 120 Ω are shown in Fig. 9 for the

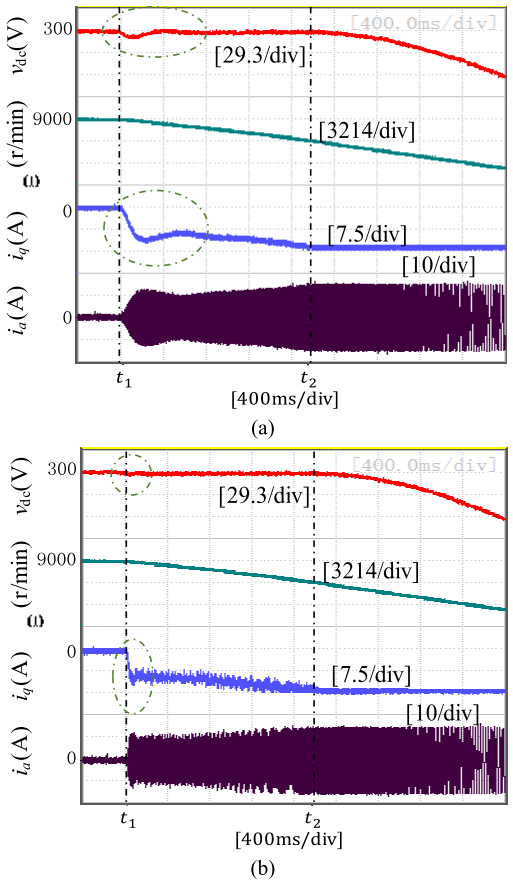

FIGURE 11. Experimental discharge waveforms with the initial speed of 9000 r/min and the impact load of 120 Ω. (a) PI controller. (b) I&IM adaptive controller.

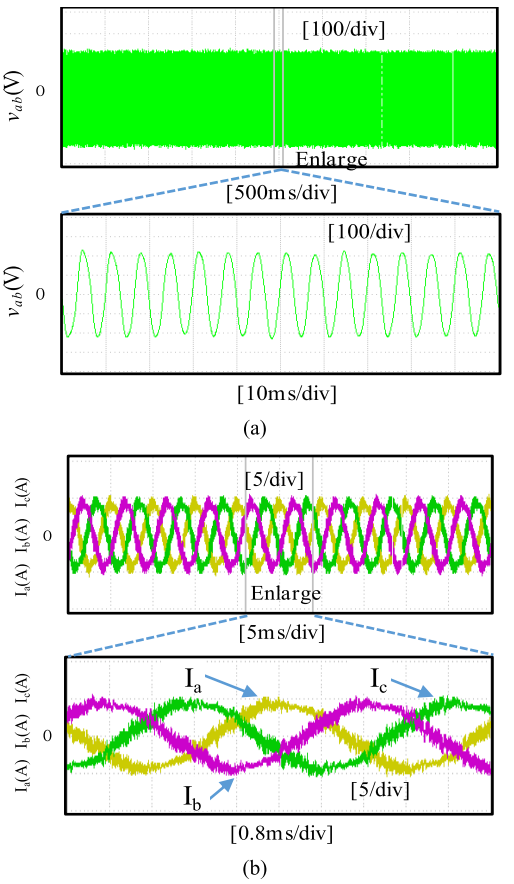

FIGURE 12. Experimental waveforms of line voltage and line current of PMSM/G with 9000 r/min. (a) line voltage. (b) line current.

traditional PI controller and the I&IM adaptive controller, respectively. It is shown that both controllers can recover to 300 V after a minor drop. The maximum voltage drops and recovery time of the PI controller is 5.8 V and 0.3 s, whereas those of the I&IM adaptive controller is 1.8 V and 0.16 s. The I&IM adaptive controller shows a better regulation ability and a more stable DC-link voltage. Since the output power of a PMSM/G is proportional to its rotational speed, when the rotational speed is lower than a minimum speed of PMSM/G in real FESS applications, the output instantaneous power of PMSM/G is lower than the load power, so the DC-link voltage drops after time t_2.

The experimental waveforms of line voltage and line current of PMSM/G are shown in Fig. 10. The waveforms of line current lags 120 degrees in turn and have good sinusoidal degree. The amplitude of line current and that of line voltage is about 5 A and 380 V, respectively.

The experimental results with the initial rotational speed of 9000 r/min are shown in Fig. 11. The maximum voltage drop and recovery time increase to 6.6 V and 0.57 s in the case of the PI controller, whereas the results are 1.9 V and 0.19 s for the I&IM adaptive controller. It is shown that the changes in the voltage drop and recovery time in the PI controller are larger than that in the I&IM adaptive controller. In theory, the reason is that the operational rotational speed and the nonlinear factor of the system are taken into account in the I&IM adaptive controller design, but ignored in the PI controller design.

The experimental waveforms of line voltage and line current of PMSM/G are shown in Fig. 12. The waveforms of line current lags 120 degrees in turn and have good sinusoidal degree. The amplitude of line current is about 5 A.

The experimental results with the initial rotational speed of 6000 r/min are shown in Fig. 13. Experimental waveforms of line voltage and line current of PMSM/G are shown in Fig. 14. The maximum voltage drops and the recovery time with the PI controller increase to 7.5 V and 0.6 s, respectively, whereas the results are 2.2 V and 0.2 s for the I&IM adaptive controller. The I&IM adaptive controller still shows a better regulation ability and a smaller change in transient performance. The waveforms of line current lags 120 degrees in turn and still have good sinusoidal degree. In practical, according to the experiment results, we draw a conclusion that value of maximum voltage drops with PI is almost four times than that with I&IM adaptive controller when the experimental prototype rig is operated at 12000, 9000, and 6000 r/min, respectively. Similarly, value of voltage recovery time with PI is almost three times than that with the I&IM adaptive controller at different rotating speed, respectively.

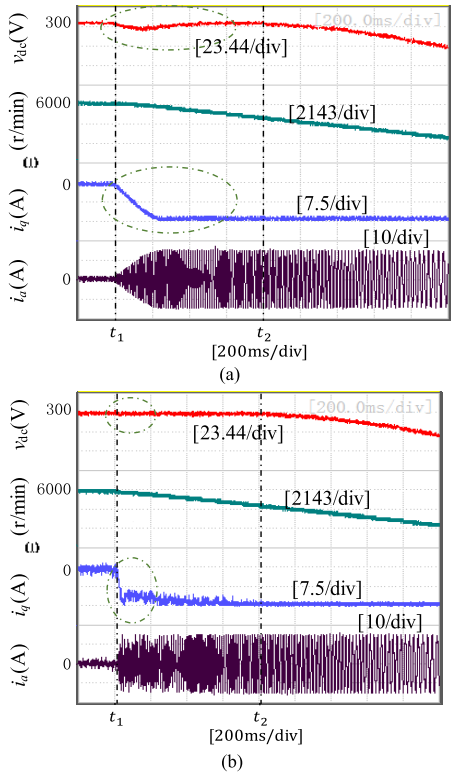

FIGURE 13. Experimental discharge waveforms with the initial speed of 6000 r/min and the impact load of 120 Ω. (a) PI controller. (b) I&IM adaptive controller.

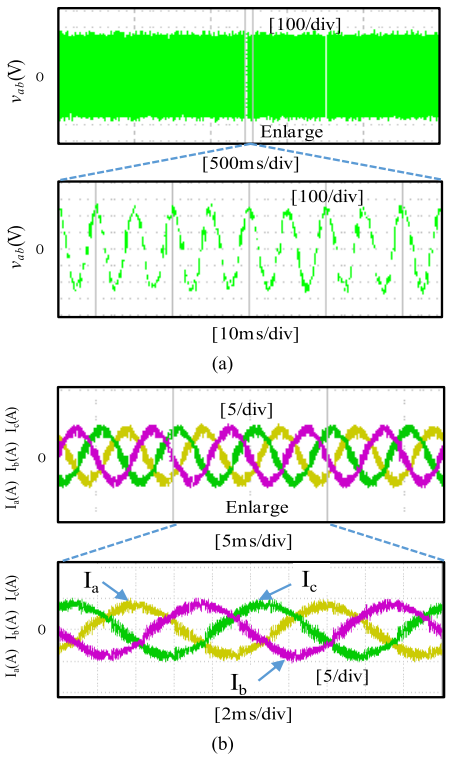

FIGURE 14. Experimental waveforms of line voltage and line current of PMSM/G with 6000 rpm. (a) line voltage. (b) line current.

The purpose of this example is to show shorter regulation ability and more stable DC-link voltage in the discharge process of the FESS using the I&IM adaptive controller at three typical initial rotational speeds of 12000, 9000 and 6000 r/min, with the impact load of 120 Ω.

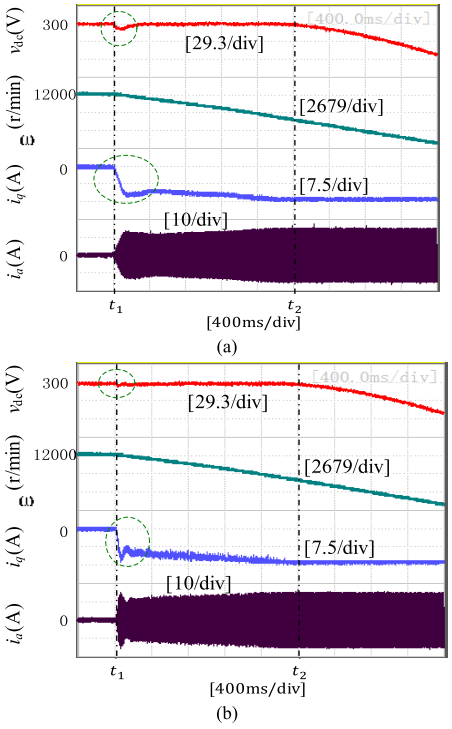

FIGURE 15. Experimental discharge waveforms with the initial speed of 12000 r/min and the impact load of 75 Ω. (a) PI controller. (b) I&IM adaptive controller.

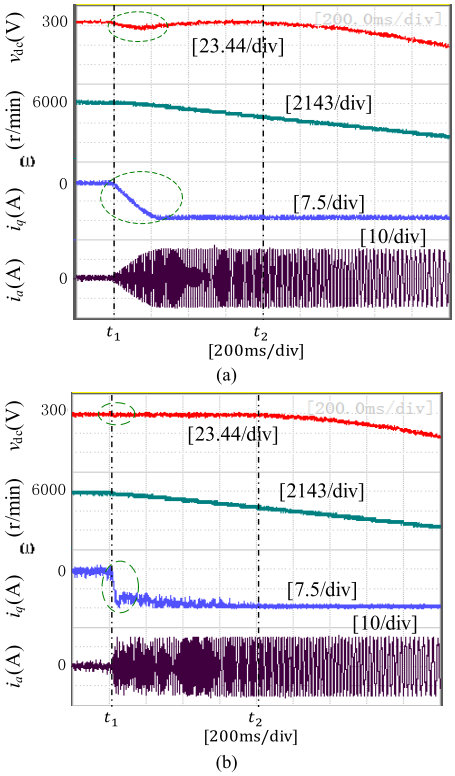

FIGURE 16. Experimental discharge waveforms with the initial speed of 6000 r/min and the impact load of 160 Ω. (a) PI controller. (b) I&IM adaptive controller.

Further, in order to verify the effectiveness of the I&IM adaptive controller as impact load varies. Fig. 15 and Fig. 16 shows the results when impact load is 75 Ω with the rotational speed of 12000 r/min and impact load is 160 Ω with the rotational speed of 6000 r/min, respectively. In Fig. 15, the maximum voltage drop and recovery time increase to 7.9 V and 0.35 s in the case of the PI controller, whereas the results are 3.7 V and 0.18 s for the I&IM adaptive controller. In Fig. 16, the maximum voltage drop (7.2 V) with the PI controller is four times higher than that (1.8 V) with the I&IM adaptive controller, and the recovery time (0.5 s) with PI controller is five times higher than that (0.1 s) with the I&IM adaptive controller. It is shown that the DC-link voltage with the PI controller and the I&IM adaptive controller can both recover to 300 V after a minor drop.

Therefore, we concluded that the proposed I&IM adaptive controller realizes a better transient performance when switching load within the wide rotational speed range from 6000 to 12000 r/min. The purpose of this example is to verify the effectiveness of the I&IM adaptive controller as impact load changes to 75 Ω, 120 Ω and 160 Ω.

Based on above results, it is shown that the I&IM adaptive control can be applied to the cooperative control problem. In particular, the control performance is much more effective when combing the I&IM adaptive controller and some optimization algorithm. For example, Deng *et al*. [34] introduced an adaptive technique, a distributed resilient control method for frequency/voltage restoration, fair real power sharing and state-of-charge balancing in MGs with multiple ESSs is proposed in the presence of actuation/propulsion faults and attacks. The stability of the proposed method is rigorously proved by Lyapunov methods. This adaptive technique could be replaced by the I&IM adaptive controller which is a nonlinear controller and has good robustness. Wang *et al*. [35] proposed a metamorphic adaptive low-gain feedback approach to investigate the semi-global robust tracking consensus problem of multi-agent uncertain systems with input saturation under a directed communication topology. In addition, Wang *et al*. [36] also proposed a multiple saturation levels framework to investigate the semi-global tracking cooperative control problem of multi-agent systems with switching communication topologies. Because the research objects of [35] and [36] are nonlinear systems, the I&IM adaptive controller is also useful to address this question.

VI. CONLUSION

This paper proposed an adaptive nonlinear controller for wide rotational speed operation of a PMSM/G based FESS. To realize the nonlinear control algorithm, the characteristic of the inner current control loop is incorporated in the dynamic equation of the DC-link voltage to form an affine nonlinear system. The control law and the adaptive law are derived by establishing a mapping relationship between the controlled plant and the desired target system using the I&IM approach. The advantage of the I&IM adaptive controller is that the convergence characteristics of the estimated parameter can be regulated quantitatively. The globally asymptotically stability of the system at the equilibrium point is verified via the Lyapunov stability theory. Theoretical analysis shows that the parameter error does not affect the position of the equilibrium point, and the experimental results verify the stability and good dynamic response of the closed-loop system within a wide rotational speed operation when using the proposed I&IM adaptive controller. In future, we will furtherly study the control strategy of the FESS, such as active control for rotor vibration and active magnetic bearing technology application including high-speed flywheel storage systems, especially in the full rotational speed range including the rigid mode frequency.

REFERENCES

[1] G. S. M. Mousavi, F. Faraji, A. Majazi, and K. Al-Haddad, "A comprehensive review of flywheel energy storage system technology," *Renew. Sustain. Energy Rev.*, vol. 67, pp. 477–490, Jan. 2017.

[2] A. A. K. Arani, H. Karami, G. B. Gharehpetian, and M. S. A. Hejazi, "Review of flywheel energy storage systems structures and applications in power systems and microgrids," *Renew. Sustain. Energy Rev.*, vol. 69, pp. 9–18, Mar. 2017.

[3] F. Nadeem, S. M. S. Hussain, P. K. Tiwari, A. K. Goswami, and T. S. Ustun, "Comparative review of energy storage systems, their roles, and impacts on future power systems," *IEEE Access*, vol. 7, pp. 4555–4585, 2019.

[4] J.-H. Choi, S.-M. Jang, S.-Y. Sung, J.-M. Kim, Y.-S. Park, Y.-J. Kim, and D.-H. Oh, "Operating range evaluation of double-side permanent magnet synchronous Motor/Generator for flywheel energy storage system," *IEEE Trans. Magn.*, vol. 49, no. 7, pp. 4076–4079, Jul. 2013.

[5] A. Ahmed, Y. Sozer, and M. Hamdan, "Maximum torque per ampere control for buried magnet PMSM based on DC-link power measurement," *IEEE Trans. Power Electron.*, vol. 32, no. 2, pp. 1299–1311, Feb. 2017.

[6] A. T. Elsayed, T. A. Youssef, and O. A. Mohammed, "Modeling and control of a low-speed flywheel driving system for pulsed-load mitigation in DC distribution networks," *IEEE Trans. Ind. Appl.*, vol. 52, no. 4, pp. 3378–3387, Jul. 2016.

[7] M. Ghanaatian and S. Lotfifard, "Control of flywheel energy storage systems in the presence of uncertainties," *IEEE Trans. Sustain. Energy*, vol. 10, no. 1, pp. 36–45, Jan. 2019.

[8] F. Diaz-Gonzalez, F. D. Bianchi, A. Sumper, and O. Gomis-Bellmunt, "Control of a flywheel energy storage system for power smoothing in wind power plants," *IEEE Trans. Energy Convers.*, vol. 29, no. 1, pp. 204–214, Mar. 2014.

[9] H. H. Abdeltawab and Y. A.-R.-I. Mohamed, "Robust energy management of a hybrid wind and flywheel energy storage system considering flywheel power losses minimization and grid-code constraints," *IEEE Trans. Ind. Electron.*, vol. 63, no. 7, pp. 4242–4254, Jul. 2016.

[10] M. Murayama, S. Kato, H. Tsutsui, S. T. Iio, and R. Shimada, "Combination of flywheel energy storage system and boosting modular multilevel cascade converter," *IEEE Trans. Appl. Supercond.*, vol. 28, no. 3, pp. 412–422, Apr. 2018.

[11] S. Ghosh and S. Kamalasadan, "An energy function-based optimal control strategy for output stabilization of integrated DFIG-flywheel energy storage system," *IEEE Trans. Smart Grid*, vol. 8, no. 4, pp. 1922–1931, Jul. 2017.

[12] L. Jarzebowicz, "Errors of a linear current approximation in high-speed PMSM drives," *IEEE Trans. Power Electron.*, vol. 32, no. 11, pp. 8254–8257, Nov. 2017.

[13] T. Tarczewski and L. M. Grzesiak, "Constrained state feedback speed control of PMSM based on model predictive approach," *IEEE Trans. Ind. Electron.*, vol. 63, no. 6, pp. 3867–3875, Jun. 2016.

[14] Y. Liu, B. Niu, F. Chu, and Y. Liu, "Adaptive fuzzy output-feedback tracking control for a class of switched stochastic nonlinear time-delay systems," *Circuits, Syst., Signal Process.*, vol. 35, no. 8, pp. 2762–2788, Oct. 2015.

[15] F. F. M. El-Sousy and K. A. Abuhasel, "Adaptive nonlinear disturbance observer using a double-loop self-organizing recurrent wavelet neural network for a two-axis motion control system," *IEEE Trans. Ind. Appl.*, vol. 54, no. 1, pp. 764–786, Jan. 2018.

[16] H. Taghavifar, A. Mardani, C. Hu, and Y. Qin, "Adaptive robust nonlinear active suspension control using an observer-based modified sliding mode interval type-2 fuzzy neural network," *IEEE Trans. Intell. Vehicles*, vol. 5, no. 1, pp. 53–62, Mar. 2020.
[17] L. Ma, X. Ning, X. Huo, and X. D. Zhao, "Adaptive finite-time output-feedback control design for switched pure-feedback nonlinear systems with average dwell time," *Nonlinear Anal-Hybri.*, vol. 37, pp. 1–23, Apr. 2020.
[18] X.-H. Chang, J. Xiong, and J. H. Park, "Estimation for a class of parameter-controlled tunnel diode circuits," *IEEE Trans. Syst., Man, Cybern. Syst.*, early access, Aug. 13, 2019, doi: 10.1109/TSMC.2018.2859933.
[19] B. H. Kenny, P. E. Kascak, R. Jansen, T. Dever, and W. Santiago, "Control of a high-speed flywheel system for energy storage in space applications," *IEEE Trans. Ind. Appl.*, vol. 41, no. 4, pp. 1029–1038, Jul. 2005.
[20] X. Chang, Y. Li, W. Zhang, N. Wang, and W. Xue, "Active disturbance rejection control for a flywheel energy storage system," *IEEE Trans. Ind. Electron.*, vol. 62, no. 2, pp. 991–1001, Feb. 2015.
[21] H. Fang, D. Wang, H. Chu, and T. Jia, "Charging and discharging control for flywheel battery driven by switched reluctance machine," in *Proc. 12th World Congr. Intell. Control Autom.*, Guilin, China, Jun. 2016, pp. 1606–1611.
[22] X. Zhang and J. Yang, "A robust flywheel energy storage system discharge strategy for wide speed range operation," *IEEE Trans. Ind. Electron.*, vol. 64, no. 10, pp. 7862–7873, Oct. 2017.
[23] X. Zhang and J. Yang, "A DC-link voltage fast control strategy for high-speed PMSM/G in flywheel energy storage system," *IEEE Trans. Ind. Appl.*, vol. 54, no. 2, pp. 1671–1679, Mar. 2018.
[24] Y. Bai, Y. Wang, M. Svinin, E. Magid, and R. Sun, "Function approximation technique based immersion and invariance control for unknown nonlinear systems," *IEEE Control Syst. Lett.*, vol. 4, no. 4, pp. 934–939, Oct. 2020.
[25] J. Keighobadi, M. Hosseini-Pishrobat, J. Faraji, and M. N. Langehbiz, "Design and experimental evaluation of immersion and invariance observer for low-cost attitude-heading reference system," *IEEE Trans. Ind. Electron.*, vol. 67, no. 9, pp. 7871–7878, Sep. 2020.
[26] B. Yi, R. Ortega, and W. Zhang, "On state observers for nonlinear systems: A new design and a unifying framework," *IEEE Trans. Autom. Control*, vol. 64, no. 3, pp. 1193–1200, Mar. 2019.
[27] A. Astolfi and R. Ortega, "Immersion and invariance: A new tool for stabilization and adaptive control of nonlinear systems," *IEEE Trans. Autom. Control*, vol. 48, no. 4, pp. 590–606, Apr. 2003.
[28] S. Monaco, D. Normand-Cyrot, and M. Mattioni, "Sampled-data stabilization of nonlinear dynamics with input delays through immersion and invariance," *IEEE Trans. Autom. Control*, vol. 62, no. 5, pp. 2561–2567, May 2017.
[29] R. Ortega, L. Praly, A. Astolfi, J. Lee, and K. Nam, "Estimation of rotor position and speed of permanent magnet synchronous motors with guaranteed stability," *IEEE Trans. Control Syst. Technol.*, vol. 19, no. 3, pp. 601–614, May 2011.
[30] N. Abou-Qamar and C. Hatziadoniu, "Cancellation of harmonic torque disturbance in permanent magnet synchronous motor drives by using an adaptive feedforward controller," *IET Power Electron.*, vol. 11, no. 14, pp. 2215–2221, Nov. 2018.
[31] V. Repecho, D. Biel, and A. Arias, "Fixed switching period discrete-time sliding mode current control of a PMSM," *IEEE Trans. Ind. Electron.*, vol. 65, no. 3, pp. 2039–2048, Mar. 2018.
[32] J. Linares-Flores, C. Garcia-Rodriguez, H. Sira-Ramirez, and O. D. Ramirez-Cardenas, "Robust backstepping tracking controller for low-speed PMSM positioning system: Design, analysis, and implementation," *IEEE Trans. Ind. Informat.*, vol. 11, no. 5, pp. 1130–1141, Oct. 2015.
[33] F. Mendoza-Mondragón, V. M. Hernandez-Guzmán, and J. Rodriguez-Reséndiz, "Robust speed control of permanent magnet synchronous motors using Two-Degrees-of-Freedom control," *IEEE Trans. Ind. Electron.*, vol. 65, no. 8, pp. 6099–6108, Aug. 2018.
[34] C. Deng, Y. Wang, C. Wen, Y. Xu, and P. Lin, "Distributed resilient control for energy storage systems in cyber-physical microgrids," *IEEE Trans. Ind. Informat.*, early access, Mar. 17, 2020, doi: 10.1109/TII.2020.2981549.
[35] B. Wang, W. Chen, and B. Zhang, "Semi-global robust tracking consensus for multi-agent uncertain systems with input saturation via metamorphic low-gain feedback," *Automatica*, vol. 67, no. 9, pp. 363–373, Feb. 2019.
[36] B. Wang, W. Chen, J. Wang, B. Zhang, and P. Shi, "Semi-global tracking cooperative control for multi-agent systems with input saturation: A multiple saturation levels framework," *IEEE Trans. Autom. Control*, early access, May 6, 2020, doi: 10.1109/TAC.2020.2991695.

LEI GONG was born in Shaanxi, China, in 1993. He received the B.S. and M.S. degrees in electrical engineering from the Xi'an University of Technology, Xi'an, China, in 2015 and 2018, respectively. He is currently pursuing the Ph.D. degree with the College of Electrical Engineering, Zhejiang University, Hangzhou, China.

His research interests include active control for rotor vibration and active magnetic bearing technology application.

MENG WANG was born in Shaanxi, China, in 1987. He received the B.S. degree in electronic and information engineering and the Ph.D. degree in electrical engineering from Zhejiang University, Hangzhou, China, in 2008 and 2017, respectively. He is currently a Researcher focused on the high-speed permanent magnet synchronous machine drive and the flywheel energy storage systems.

CHANGSHENG ZHU was born in Shaanxi, China, in August 1963. He received the B.S. and M.S. degrees in aeroengines from Northwestern Polytechnical University, Shaanxi, in 1983 and 1986, respectively, and the Ph.D. degree in chemical process machinery from Zhejiang University, Hangzhou, China, in 1992.

He is currently a Professor with the College of Electrical Engineering, Zhejiang University. His research interests include active magnetic bearings, high-speed flywheel storage systems, high-speed motors, rotor dynamics and control, and vibration and noise of electric machines.